Nanotechnology

PAPER

Stability and electronic properties of hybrid SnO bilayers: SnO/graphene and SnO/BN

To cite this article: Qing Guo *et al* 2017 *Nanotechnology* **28** 475708

View the article online for updates and enhancements.

This content was downloaded from IP address 141.219.152.23 on 03/11/2017 at 14:58

Nanotechnology 28 (2017) 475708 (7pp) https://doi.org/10.1088/1361-6528/aa92ab

Stability and electronic properties of hybrid SnO bilayers: SnO/graphene and SnO/BN

Qing Guo[1], Gaoxue Wang[1], Ashok Kumar[2] and Ravindra Pandey[1]

[1] Department of Physics, Michigan Technological University, Houghton, Michigan 49931, United States of America
[2] Centre for Physical Sciences, Central University of Punjab, Bathinda, Punjab 151001, India

E-mail: pandey@mtu.edu

Received 7 August 2017, revised 27 September 2017
Accepted for publication 11 October 2017
Published 3 November 2017

Abstract

Van der Waals structures based on two-dimensional materials have been considered as promising structures for novel nanoscale electronic devices. Two-dimensional SnO films which display intrinsic p-type semiconducting properties were fabricated recently. In this paper, we consider vertically stacked heterostructures consisting of a SnO monolayer with graphene or a BN monolayer to investigate their stability, electronic and transport properties using density functional theory. The calculated results find that the properties of the constituent monolayers are retained in these SnO-based heterostructures, and a p-type Schottky barrier is formed in the SnO/graphene heterostructure. Additionally, the Schottky barrier can be effectively controlled with an external electric field, which is useful characteristic for the van der Waals heterostructure-based electronic devices. In the SnO/BN heterostructure, the electronic properties of SnO are least affected by the insulating monolayer suggesting that the BN monolayer would be an ideal substrate for SnO-based nanoscale devices.

Supplementary material for this article is available online

Keywords: 2D materials, Van der Waals heterostructure, tin monoxide

(Some figures may appear in colour only in the online journal)

1. Introduction

Two-dimensional (2D) materials exhibit novel nanoscale properties for next-generation electronic devices. Additionally, structures consisting of two or more 2D materials interacting via the van der Waals (vdW) forces provide a unique way of fabricating heterojunctions which can be used as building blocks in a variety of nanoscale devices [1]. For example, the phosphorene/graphene heterostructure displays tuning of the contact from n-type Schottky to p-type Schottky and then ohmic by simply tailoring the relative position of the graphene's Fermi level within the phosphorene's band gap [2]. Additional examples of such heterostructures include semiconducting transition metal dichalcogenides and graphene, which are proposed for large-scale 2D electronics [3–9]. Note that synthesis and characterization of such heterostructures involving graphene is of particular interest due to graphene being a material with a high electron mobility [10].

Tin monoxide (SnO), unlike most other oxide semiconductors, shows intrinsic p-type semiconductor character due to the presence of an unintended Sn vacancy [11, 12]. Bulk SnO has a tetragonal PbO layered structure with the space group of $P4/nmm$. In the corresponding single-layer structure, oxygen atoms are at the middle plane, while each Sn atom forms a pyramid structure with the four neighboring O atoms. These pyramids alternatively distribute on both sides of the SnO layered structure (figure S1 is available online at stacks.iop.org/NANO/28/475708/mmedia). Properties like intrinsic p-type conduction and a large optical band gap have generated significant interest in this novel 2D material [11, 13–20]. For example, this material can be used to produce high-performance p-channel thin-film transistors (TFTs) [14]; double layers of SnO under suitable strain could be a promising catalyst for photocatalytic water splitting[16]; its monolayer's multiferroic properties can be controlled by hole density [17]; and SnO sheets can be promising materials

 © 2017 IOP Publishing Ltd Printed in the UK

for sodium ion battery (SIB) applications [18]. In multilayered SnO films with intrinsic p-type semiconducting properties, the direct optical band gap is measured to vary from 3.53 eV to 2.80 eV in going from two to nine layers in thickness [19]. The band gap of the bulk-like film is 2.95 eV [16]. Recently, p-n heterojunctions consisting of SnO and MoS_2 layers have been successfully fabricated [21].

In this paper, we investigate the feasibility of forming 2D heterostructures of SnO/graphene or SnO/BN monolayers focusing on their stability and electronic properties. Specifically, we will ask the questions: can a SnO monolayer form a vdW heterostructure with graphene or a BN monolayer? If such a heterostructure is stable, can it display characteristics of a typical p-type or n-type heterojunctions under the application of an external electric field? Employing density functional theory, we will first calculate the properties of a monolayer and bilayers of SnO to establish a reference point for SnO heterostructures formed with graphene or BN monolayers. Next, the structural stability and electronic properties of SnO/graphene and SnO/BN heterostructures will be determined. Finally, the effect of an external electric field applied perpendicular to the heterostructure will be investigated to ascertain the properties of the heterojunctions formed by the constituent monolayers.

2. Computational methods

Electronic structure calculations were carried out within the framework of the density functional theory (DFT) by using the Vienna *Ab initio* Simulation Package (VASP) program [22, 23]. The generalized-gradient approximation (GGA) proposed by Perdew–Burk–Ernzerhof (PBE) [24] together with Grimme's D2 method [25] representing the vdW interaction term were employed. The energy convergence was set to 10^{-7} eV and the kinetic energy cut-off was 520 eV. The geometry optimization was considered to be converged when the residual force on each atom was smaller than 0.01 eV $Å^{-1}$. The reciprocal space was sampled by a grid of ($13 \times 7 \times 1$) k points for the structural optimization calculations. A larger ($33 \times 17 \times 1$) k-point grid was used for calculations of electronic properties including density of states (DOS) and band structure. In the periodic supercell calculations of heterostructures, the vacuum distance normal to the plane was larger than 14 Å to eliminate interaction between the replicas.

To test the reliability of our modeling elements, we first performed calculations on the bulk SnO. The calculated structural parameters for the bulk SnO agree very well with the corresponding experimental [19, 26] and the previously reported theoretical studies [12, 27–31] (table S1). For example, the calculated lattice constants, a and c, are 3.835 Å and 4.817 Å, respectively, as compared to the corresponding experimental values 3.801 Å and 4.835 Å for the bulk SnO. The calculated interlayer distance is 2.68 Å. We find that the inclusion of vdW interactions via the D2 term in calculations appear to be important for the bulk SnO as it increases the interlayer binding energy from 0.15 eV to 0.73 eV per SnO unit cell, and yields a more accurate interlayer distance of 2.48 Å as compared to the experimental value of 2.52 Å.

3. Results and discussions

3.1. Equilibrium configuration and stability

To find the energetically preferred stacking configurations for heterostructures, the registry index (RI) model was initially used. The RI model employs simple geometric considerations to obtain energetically preferred configurations of a multilayer system with modest computational resources [32]. The stability is defined by the binding energy obtained from the RI index which, in turn, is proportional to the projected overlap area between the adjacent atoms at the interface of the heterostructure (figures S2 and S3). The RI configurations for the SnO-based heterostructures are then taken as initial configurations for the DFT calculations. Following the stacking nomenclature of graphite, we define the stacking configurations to be AA (i.e. one of the bottom Sn atoms is on top of a C atom of graphene) and AB (i.e. one of the bottom Sn atoms is located over the hollow site of the hexagonal lattice) as displayed in figure 1.

For the SnO/graphene heterostructure, the DFT results find the AB-stacked configuration to be preferred with the binding energy of 0.24 eV/SnO unit cell and the interlayer distance of 3.42 Å. The bond distances $R_{Sn\text{-}O}$ and $R_{C\text{-}C}$ are 2.35 (2.24) and 1.42 (1.41) Å in x- (y-) direction, respectively. The AA-stacked configuration is slightly higher in energy with the binding energy of 0.23 eV/SnO unit cell and the interlayer distance of 3.47 Å. Replacement of graphene with the BN monolayer in the heterostructure also yields the AB-stacked configuration to be energetically preferred with the binding energy of 0.29 eV/SnO unit cell and the interlayer distance of 3.36 Å. Note that calculations for the SnO bilayer find the AA-stacked configuration to be energetically preferred with the interlayer distance of 2.50 Å and the binding energy of 0.35 eV/unit cell (figure S4, and table S2), which follows the structure of bulk SnO. The calculated lattice constant is 3.84 Å with the $R_{Sn\text{-}O}$ bond distance of 2.25 Å for the SnO bilayer.

3.2. Electronic properties

For the SnO/graphene heterostructure, the calculated band structure and density of states (DOS) are displayed in figure 2. The band structure of the heterostructure shows features of the constituent monolayers including Dirac-cone points of graphene (red dots) and direct/indirect band gaps of the SnO monolayer. A small band gap of about 8 meV is opened up in graphene suggesting a small but noticeable degree of the interlayer coupling in the heterostructure.

The band alignments of graphene, BN, SnO and the corresponding heterostructures are summarized in figure 3. Overall, the band alignments in the heterostructures are comparable to the constituent monolayers, indicating the presence of the weak vdW interactions between monolayers in the heterostructure. Interestingly, we notice that a Schottky barrier is formed in the heterostructure of SnO and graphene. According to the Schottky–Mott model at the interface between a metal and a semiconductor, the Schottky barrier is

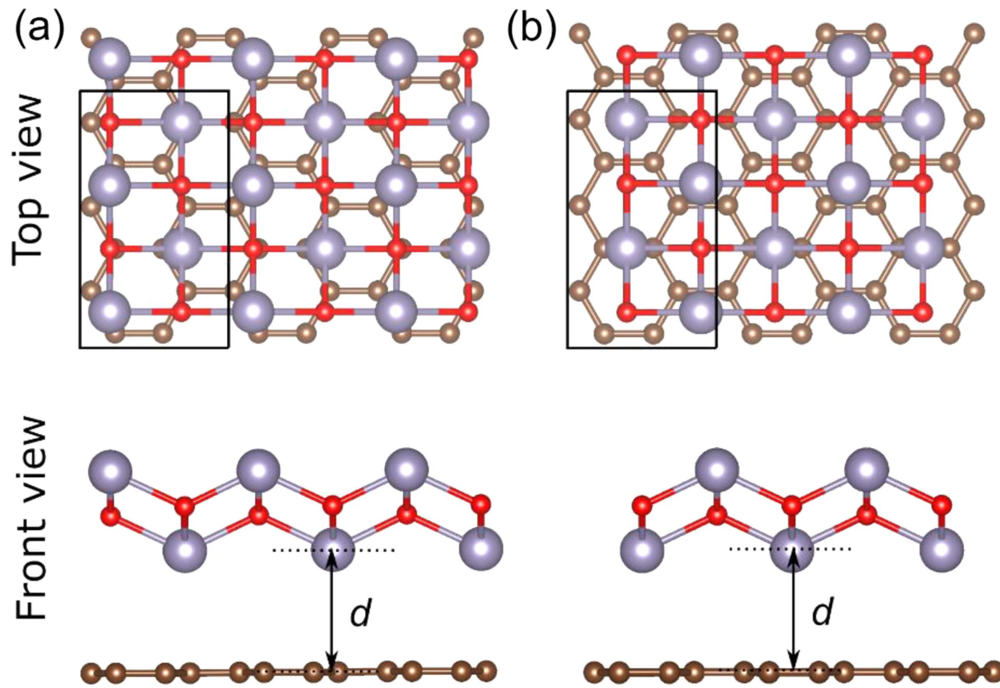

Figure 1. A schematic diagram of the (a) AA- and (b) AB-stacking configurations of the SnO/graphene heterostructure. The red, grey and brown balls represent O, Sn and C atoms, respectively.

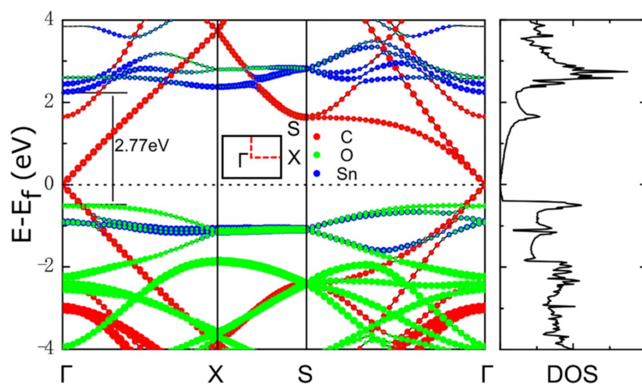

Figure 2. SnO/graphene heterostructure: calculated band structure and total density of states. The bands projected to C, Sn and O atoms are displayed by red, blue and green dots, respectively.

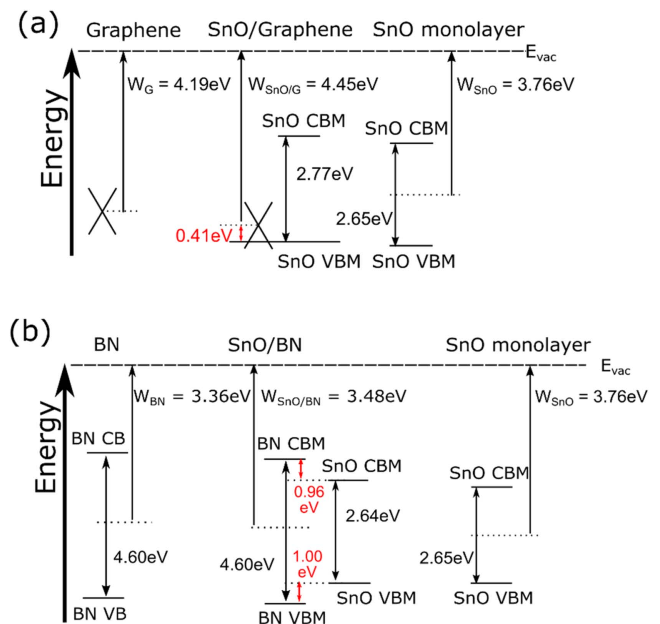

Figure 3. (a) Band alignments of graphene, SnO monolayer and SnO/graphene bilayer with respect to the vacuum level. (b) Band alignments of energy levels of graphene, SnO monolayer and SnO/BN bilayer with respect to the vacuum level. The black cone represents the Dirac point of graphene. SnO-VBM and SnO-CBM are valence band and conduction band edges of SnO with respect to the vacuum level, respectively. W_G, W_{SnO}, $W_{SnO/G}$ and $W_{SnO/BN}$ are the work functions of graphene, SnO monolayer, SnO/graphene and SnO/BN, respectively.

defined as the energy difference between the Fermi level of the metal and the conduction band minimum (CBM) or valence band maximum (VBM) of the semiconductor. If the Fermi level of the metal is closer to the CBM, an n-type Schottky barrier is formed. Otherwise, a p-type Schottky barrier is formed.

In the case of the SnO/graphene heterostructure, the Fermi level of graphene is closer to the VBM of the SnO monolayer (figure 2) that results into a p-type Schottky barrier with a height of 0.41 eV as illustrated in figure 3(a). Additional calculations were also performed to illustrate the change in Schottky barrier height with the increasing thickness of the oxide layer. The results find that the Schottky barrier height decreases from 0.41 eV for SnO monolayer to 0.10 eV for SnO bilayer and 0.11 eV for SnO trilayer in the SnO-based heterostructures (figure S6). For the SnO/BN heterostructure, the band structure and values of band energies (figure 3(b), figure S7) of the SnO monolayer have not been modified by the BN monolayer, implying that the insulating BN monolayer can be an ideal substrate for SnO-based electronic devices.

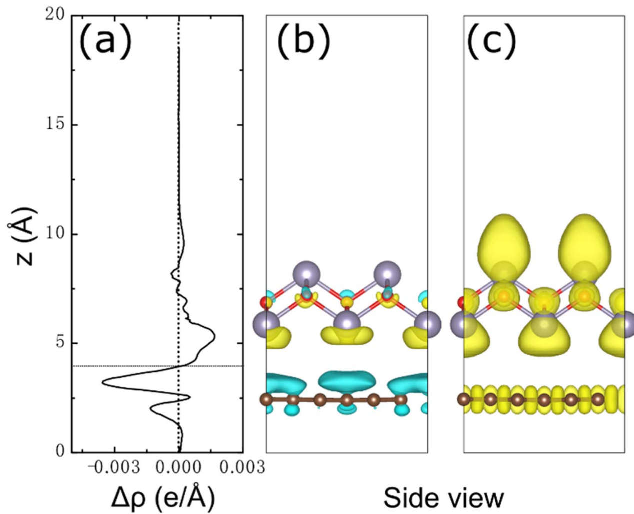

Figure 4. (a) The profile of the planar average charge density difference as a function of position along the *z*-direction. The horizontal dashed line denotes the central location between SnO layer and graphene. (b) A side view of the charge density difference with the isosurface value of 0.0002 e/Å^3. (The yellow and blue colors represent electron-rich and electron-deficient regions, respectively.) (c) Electron localization function (ELF) of the SnO/graphene heterostructure with the isosurface value of 0.8.

In the heterostructure, an unambiguous signature of the interlayer coupling can be seen in the charge density difference plots displayed in figure 4. The electron localization function (ELF) plot (figure 4(c)) shows an asymmetric ELF sphere, further suggesting existence of the interfacial interaction in the heterostructure. The ELF sphere is associated with the lone pair of a Sn atom formed due to coupling between Sn ($5p_z$) orbital and the anti-bonding Sn (5s)–O ($2p_z$) hybridized orbitals (figure S9) [12].

To affirm the cause of opening of the band gap in graphene due to the presence of the oxide monolayer, we performed calculations with a shorter interlayer spacing of 2.62 Å to mimic the strengthening of the interaction between the individual monolayers in the heterostructure. This has resulted in a noticeable opening of the band gap of graphene to 27 meV without modifying broad features of the band structure of the heterostructure (figure S5).

For the SnO/BN heterostructure, the constituent monolayers retain their individual features in the band structure. The minimum band gap of 2.6 eV is found to be associated with the SnO monolayer since the BN monolayer has a large band gap of 4.6 eV (figure S7). Note that the structural property of the h-BN monolayer is similar to that of graphene.

It is to be noted that the DFT calculations for the SnO-based heterostructures were performed in the context of the 'commensurate lattice approximation' where graphene was used as a reference lattice. Initially, a (1 × 3) cell for graphene and a (1 × 2) cell for the SnO monolayer were used in the periodic supercell simulating the heterostructure. Due to lattice mismatch between the SnO monolayer and graphene, the oxide monolayer is elongated in the *x*-direction and is shortened in the *y*-direction. The calculated lattice constant ($a = b$) of the pristine SnO monolayer is 3.81 Å, and the values of a and b for graphene are 4.26 Å and 2.46 Å, respectively.

To understand the effect of lattice mismatch in the heterostructure, a larger supercell consisting of a (7 × 3) cell for graphene and a (8 × 2) cell for the SnO monolayer was considered (figure S8). We find that the structural properties are nearly converged; the interlayer distance is 3.42 Å (3.50 Å) and the binding energy value is 40 meV/C atom (41 meV/C atom) for the small (large) supercell. Likewise, we find a similarity in their band structures (figure S8). In the following, we therefore present the results associated with the smaller supercell simulating the SnO/graphene heterostructure. Note that heterostructures with noticeable lattice mismatch have been fabricated including phosphorene/graphene [2] and WSe_2/graphene [33].

3.3. Effect of an external electric field

To consider the effect of a gate field on the electronic properties of a heterostructure in a device configuration, calculations in the presence of an external electric field were performed in which the forward direction of the electric field was taken from the oxide monolayer to graphene.

Figure 5 displays the calculated band structures in the presence of the electric field applied perpendicular to the heterostructure. The results show that application of the positive electric field shifts SnO-CBM to the lower values relative to the Dirac point (the red line in figure 5(b)). On the other hand, SnO-VBM moves away from the Dirac point as shown by the blue line in figure 5 (b). This movement of the band edges led to conversion of the p-type Schottky barrier to n-type with electric field at 0.7 eV/Å. When a negative electric field is applied, SnO-VBM touches the Fermi level with electric field larger than 0.5 eV Å^{-1} making the heterojunction ohmic. Note that obtaining zero or even very low Schottky barrier in heterojunctions is very important for the realization of the high-performance field-effect transistors (FETs) [34]. Tuning of the contact type can therefore be achieved by the external electric field applied to the SnO/graphene heterostructure.

3.4. Electronic transport properties: calculations of tunneling currents

Next, we use a conventional setup mimicking the scanning tunneling microscope (STM) experiments to calculate the tunneling current from the sample to the tip at location $\vec{r}_t$ based on the Tersoff and Hamann approximation [35]:

$$I(\vec{r}_t;\, V) \approx \frac{2\pi e}{\hbar}\int_{-\infty}^{+\infty} \rho_t\left(E - \frac{eV}{2}\right)\rho_s\left(\vec{r}_t;\, E + \frac{eV}{2}\right)F(E)\mathrm{d}E, \qquad (1)$$

where ρ_t is the electron density of the tip and ρ_s is the electron density of the sample at the location of the tip. $F(E)$ is a term to include the effect of thermally excited electrons as proposed by He *et al* [36]. This approach has been successfully used to investigate the tunneling characteristics of several nanomaterials including PbS quantum dots, MoS_2 and BN

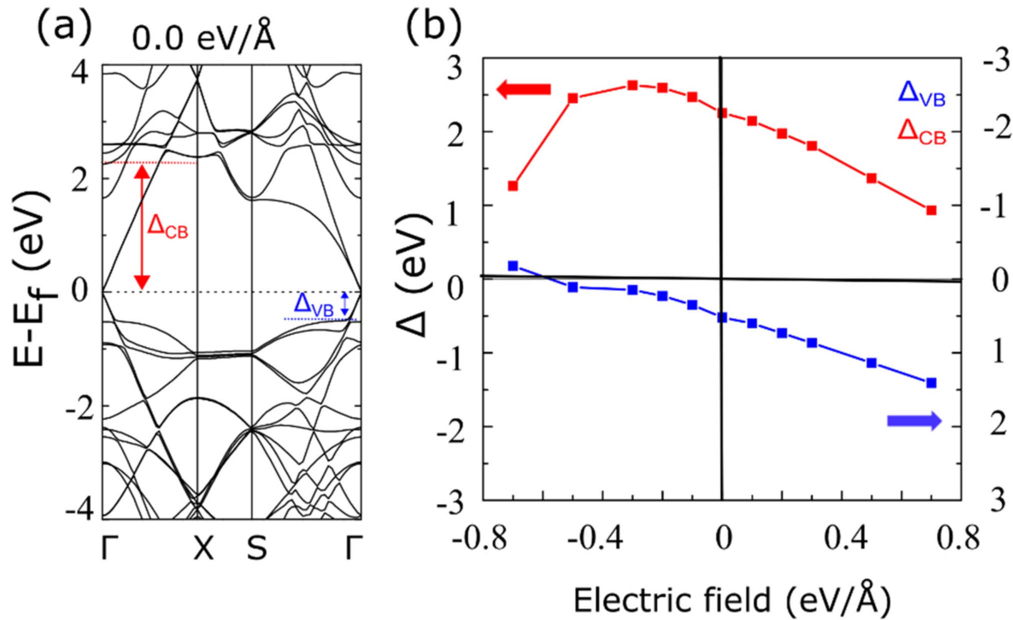

Figure 5. SnO/graphene heterostructure: The band structures calculated for EF = 0 eV Å^{-1}. (b) Variation of SnO-VBM (blue) and SnO-CBM (red) with applied electric field.

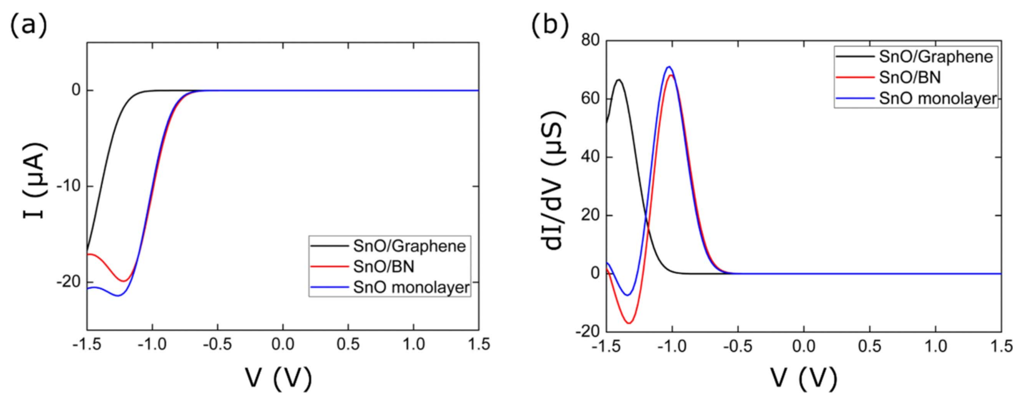

Figure 6. (a) The current–voltage characteristics and (b) the calculated differential conductance curve of SnO monolayer, SnO/graphene and SnO/BN heterostructures.

monolayers, and phosphorene by our group [37–39]. The cap of the tip used in the STM measurements was simulated by a Au_{13} cluster in our calculations.

The calculated tunneling currents associated with the heterostructures together with that of the oxide monolayer are plotted in figure 6 over the range of external bias between -1.5 V and $+1.5$ V. It is important to note that the tunneling current is an integration of the convolution of DOS of the tip and the sample, and will depend on the filled and unfilled electron states near the Fermi energy of a given system. Also, the magnitude of the current will depend on the tip–monolayer distance which will not, however, influence the trends in the I-V characteristics predicted in figure 6.

For the pristine SnO monolayer, the threshold voltage is about -0.5 V and thereafter an approximately linear relationship of the tunneling current versus voltage is seen. This is also the case with the heterostructures, though the threshold voltage of SnO/graphene (≈ -0.9 V) is slightly higher than that of the SnO/BN heterostructure (≈ -0.5 V). The presence of a BN monolayer does not modify the I-V characteristics of the SnO monolayer, however, a clear shift toward negative bias is predicted for SnO/graphene due to the change of its Fermi level. Figure 6(a) also displays the negative differential resistance (NDR) effect at about -1.3 V for the SnO monolayer and the SnO/BN heterostructure, which is also confirmed by differential conductance curves shown in figure 6(b). This small, but noticeable NDR effect appears to be associated with an overlap of the density of states of tip and SnO in these heterostructures (figure S10).

To characterize the topography of the SnO-based heterostructures, we now show the simulated STM images generated from the position-projected tunneling currents (figure 7). In simulations, we have used the constant current mode with the tip moving over the surface. The STM images show similar characteristics with the bright regions forming a rectangular pattern which is consistent with the geometrical configuration of the SnO monolayer. Note that the bright regions correspond to the top-most Sn atoms in the heterostructures.

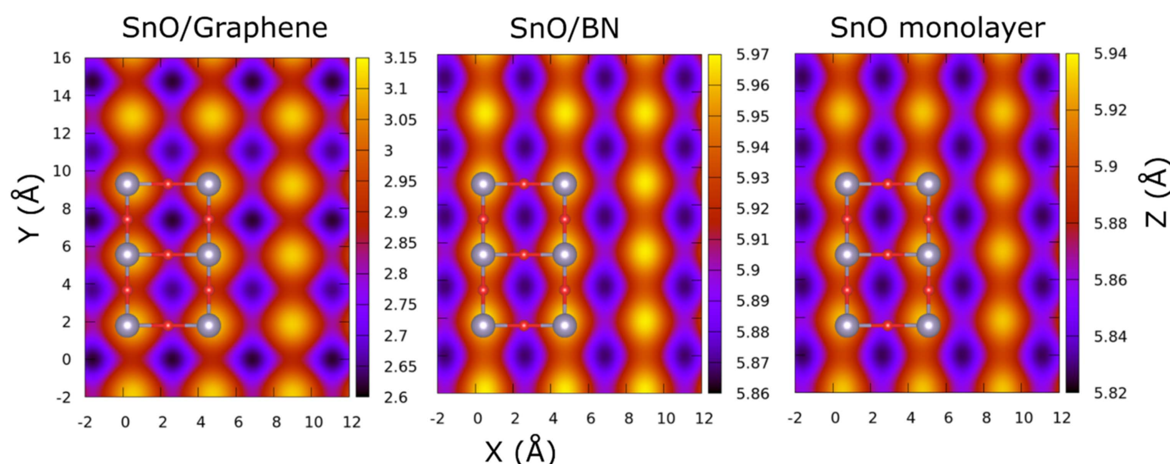

Figure 7. The STM images at constant current (0.3 nA, 1 V) of (a) SnO/graphene. (b) SnO/BN heterostructures and (c) SnO monolayer.

In 2D materials, it is generally known that the excitonic effect is important due to the anti-screening effect and the relatively large effective mass. Calculations were performed using the HSE functional form [40] which finds the band gap to be 3.7 eV for the SnO monolayer. Following the work of Jiang *et al* [41] one can then approximate the exciton binding energy to be 0.93 eV. Note that a linear scaling law between the quasiparticle band gap and the exciton binding energy for 2D materials has previously been suggested [41].

There exists a possibility of fabricating SnO-based heterostructures since graphene heterostructures with phosphorene [2] and WSe_2 [33] have been fabricated, for which the calculated binding energy values are 60 and 54 meV/C atom, respectively. In the present case, the calculated binding energy of the SnO/graphene heterostructure is 40 meV/C atom. Also, vdW 2D heterostructures consisted of graphene and MoS_2 monolayers have been fabricated, though there exists a lattice mismatch between graphene and MoS_2. The lattice constants of MoS_2 and graphene are 3.15 Å and 2.46 Å, respectively [21].

4. Summary

In summary, we have investigated the structure and electronic properties of the SnO/graphene and SnO/BN heterostructures by using density functional theory. We show that the electronic properties of the SnO monolayer are preserved when it is placed on the top of graphene or a BN monolayer. In the heterostructures, an external electric field can manipulate the SnO monolayer band structure relative to the graphene's Dirac point, and turn this p-type junction into n-type with positive bias and to ohmic contact with negative bias.

Acknowledgments

Helpful discussions with Kevin Waters and Max Seel are acknowledged. RAMA and Superior, high-performance computing clusters at Michigan Technological University, were used in obtaining results presented in this paper. Support from Dr S Gowtham is gratefully acknowledged.

ORCID iDs

Ravindra Pandey https://orcid.org/0000-0002-2126-1985

References

[1] Geim A K and Grigorieva I V 2013 Van der Waals heterostructures *Nature* **499** 419–25
[2] Padilha J E, Fazzio A and da Silva A J 2015 Van der Waals heterostructure of phosphorene and graphene: tuning the Schottky barrier and doping by electrostatic gating *Phys. Rev. Lett.* **114** 066803
[3] Pierucci D *et al* 2016 Band alignment and minigaps in monolayer MoS2-graphene van der Waals heterostructures *Nano Lett.* **16** 4054–61
[4] Yu L *et al* 2014 Graphene/MoS2 hybrid technology for large-scale two-dimensional electronics *Nano Lett.* **14** 3055–63
[5] Roy K *et al* 2013 Graphene-MoS2 hybrid structures for multifunctional photoresponsive memory devices *Nat. Nanotechnol.* **8** 826–30
[6] Kwak J Y *et al* 2016 Long wavelength optical response of graphene-MoS2 heterojunction *Appl. Phys. Lett.* **108** 091108
[7] Pandey T *et al* 2016 Pressure-induced charge transfer doping of monolayer graphene/MoS2 heterostructure *Small* **12** 4063–9
[8] Britnell L *et al* 2013 Strong light–matter interactions in heterostructures of atomically thin films *Science* **340** 1311–4
[9] Xu L *et al* 2017 Two-dimensional MoS2-graphene-based multilayer van der Waals heterostructures: enhanced charge transfer and optical absorption, and electric-field tunable Dirac point and band gap *Chem. Mater.* **29** 5504–12
[10] Novoselov K S *et al* 2004 Electric field effect in atomically thin carbon films *Science* **306** 666–9
[11] Togo A *et al* 2006 First-principles calculations of native defects in tin monoxide *Phys. Rev.* B **74** 195128
[12] Walsh A and Watson G W 2004 Electronic structures of rocksalt, litharge, and herzenbergite SnO by density functional theory *Phys. Rev.* B **70** 235114
[13] Hosono H *et al* 2011 Bipolar conduction in SnO thin films *Electrochemical and Solid-State Letters* **14** H13–6

[14] Ogo Y *et al* 2008 p-channel thin-film transistor using p-type oxide semiconductor, SnO *Appl. Phys. Lett.* **93** 032113
[15] Ogo Y *et al* 2009 Tin monoxide as an s-orbital-based p-type oxide semiconductor: Electronic structures and TFT application *Phys. Status Solidi* (a) **206** 2187–91
[16] Zhou W and Umezawa N 2015 Band gap engineering of bulk and nanosheet SnO: an insight into the interlayer Sn-Sn lone pair interactions *Phys. Chem. Chem. Phys.*. **17** 17816–20
[17] Seixas L *et al* 2016 Multiferroic two-dimensional materials *Phys. Rev. Lett.* **116** 206803
[18] Zhang F *et al* 2017 Two-dimensional SnO anodes with a tunable number of atomic layers for sodium ion batteries *Nano Lett.* **17** 1302–11
[19] Saji K J *et al* 2016 2D tin monoxide-an unexplored p-type van der waals semiconductor: material characteristics and field effect transistors *Advanced Electronic Materials* **2** 1500453
[20] Wang Z *et al* 2016 Hybrid van der Waals p-n Heterojunctions based on SnO and 2D MoS2 *Adv. Mater.* **28** 9133–41
[21] Wang Z *et al* 2016 Hybrid van der Waals p-n heterojunctions based on SnO and 2D MoS_2 *Adv. Mater.* **28** 9133–41
[22] Kresse G and Furthmüller J 1996 Efficient iterative schemes for *ab initio* total-energy calculations using a plane-wave basis set *Phys. Rev.* B **54** 11169–86
[23] Kresse G and Furthmüller J 1996 Efficiency of ab-initio total energy calculations for metals and semiconductors using a plane-wave basis set *Comput. Mater. Sci.* **6** 15–50
[24] Perdew J P, Burke K and Ernzerhof M 1996 Generalized gradient approximation made simple *Phys. Rev. Lett.* **77** 3865–8
[25] Grimme S Semiempirical GGA-type density functional constructed with a long-range dispersion correction *J. Comput. Chem.* 2006 **27** 1787–99
[26] Moreno M S and Mercader R C 1994 Mössbauer study of SnO lattice dynamics *Phys. Rev.* B **50** 9875–81
[27] Meyer M *et al* 1998 Electronic structure of stannous oxide *Comput. Mater. Sci.* **10** 319–24
[28] Christensen N, Svane A and Blancá E P Y 2005 Electronic and structural properties of SnO under pressure *Phys. Rev.* B **72** 014109
[29] McLeod J *et al* 2011 Nature of the electronic states involved in the chemical bonding and superconductivity at high pressure in SnO *JETP Lett.* **94** 142–6
[30] Govaerts K *et al* 2013 van der Waals bonding and the quasiparticle band structure of SnO from first principles *Phys. Rev.* B **87** 235210
[31] Chen P-J and Jeng H-T 2015 Phase diagram of the layered oxide SnO: GW and electron-phonon studies *Sci. Rep.* **5** 16359
[32] Hod O 2012 Interlayer commensurability and superlubricity in rigid layered materials *Phys. Rev.* B **86** 075444
[33] Yu Z G, Zhang Y-W and Yakobson B I 2016 Strain-robust and electric field tunable band alignments in van der Waals WSe2–graphene heterojunctions *The Journal of Physical Chemistry* C **120** 22702–9
[34] Kwon J *et al* 2017 Thickness-dependent Schottky barrier height of MoS2 field-effect transistors *Nanoscale* **9** 6151–7
[35] Tersoff J and Hamann D R 1983 Theory and application for the scanning tunneling microscope *Phys. Rev. Lett.* **50** 1998–2001
[36] He H *et al* 2006 Spin-polarized electron transport of a self-assembled organic monolayer on a Ni(111) substrate: An organic spin switch *Phys. Rev.* B **73** 195311
[37] Loh G *et al* 2015 MoS2 quantum dot: effects of passivation, additional layer, and h-BN substrate on its stability and electronic properties *The Journal of Physical Chemistry* C **119** 1565–74
[38] Wang G, Pandey R and Karna S P 2015 Phosphorene oxide: stability and electronic properties of a novel two-dimensional material *Nanoscale* **7** 524–31
[39] Gupta S K *et al* 2013 Electron tunneling characteristics of a cubic quantum dot,(PbS) 32 *The Journal of Chemical Physics* **139** 244307
[40] Krukau A V *et al* 2006 Influence of the exchange screening parameter on the performance of screened hybrid functionals *J. Chem. Phys.* **125** 224106
[41] Jiang Z *et al* 2017 Scaling universality between band gap and exciton binding energy of two-dimensional semiconductors *Phys. Rev. Lett.* **118** 266401